

# Numerical study of simple shear dense granular flow of frictional elongated and flattened particles

Jacopo Bilotto<sup>1,\*</sup>, Martin Trulsson<sup>2</sup>, and Jean-François Molinari<sup>1</sup>

<sup>1</sup>Institute of Civil Engineering, Institute of Materials, École Polytechnique Fédérale de Lausanne, CH 1015 Lausanne, Switzerland

<sup>2</sup>Computational Chemistry, Lund University, Lund SE-221 00, Sweden

**Abstract.** Non-spherical particles play a crucial role in industrial and geological flows, however, a comprehensive description of their rheology as a function of inertial number and asphericity remains incomplete. In this study, we examine the influence of particle shape using spheroidal particles through simulations of simple shear flow under Lees-Edwards boundary conditions, focusing on the dense flow regime at constant applied pressure. Highly flattened, *i.e.* oblate lentil-like, particles manifest significantly fewer contacts and lower volume fraction, compared to elongated *i.e.* prolate rice-like, ones with the same shape ratio. The effective friction shows a non-monotonic dependence on the aspect ratio, and slightly flattened spheroids display a negative first normal stress difference. Furthermore, non-spherical particles tend to align their major axis with the flow, and energy dissipation becomes localized along this direction. As asphericity increases, tangential forces contribute increasingly to the overall shear stress.

## 1 Introduction

Granular materials exhibit complex mechanical behavior influenced by particle shape, which plays a crucial role in packing, compression, and shear properties [1–3].

In simple shear, spheres follow well-characterized flow laws [4], while spheroids [5], rods [6], flat disks [7], ellipses [8] and sphero-cylinders [9] demonstrate unique properties such as alignment and transmission of anisotropic stress. Furthermore, studies on elongated grains highlight the role of tangential forces in energy dissipation and shear strength enhancement [10].

Models have been developed to extend the classical  $\mu(I)$ -rheology [11] to also incorporate particle anisotropy [12, 13], with efforts to link microscopic interactions to macroscopic flow behavior. However, current models apply only to frictionless particles.

This numerical study investigates the shear flow of frictional spheroidal grains. The corresponding  $\mu(I)$ -rheology is found to vary as a function of the asphericity, with a slight dependency on particles' elongation or flattening. By analyzing shear-induced alignment, force distribution, and power dissipation, we provide new insights into shape-dependent granular mechanics, focusing on the effects of out-of-plane particle dimensions in quasi-2D flows.

## 2 Simulation set-up

All simulations are conducted using the open-source software LIGGGHTS [14]. We achieve simple shear flow in a 3D triclinic box with periodic boundaries in the flow

( $x$ ) and vorticity ( $z$ ) directions and Lees-Edwards conditions in the gradient ( $y$ ) direction. Spheroids are modeled using superquadric particles [15] with Hertz-Mindlin interaction, and Coulomb friction law. The time-step is determined from the smallest characteristic time-scale, in our case either the Hertzian collision time or the Rayleigh time, and set to 15% of this value.

We simulate  $N = 2000$  particles with approximately 12 particles per dimension and 20% polydispersity in the smallest semi-axis while keeping the aspect ratio fixed. Stress tensor components are computed using the virial stress formula:

$$\sigma_{ij} = \frac{1}{2\Omega} \sum_{k,l \in \Omega}^N (r_j^{(k)} - r_j^{(l)}) F_i^{(lk)}, \quad (1)$$

where  $\Omega$  is the system volume,  $\mathbf{r}^m$  the particle position, and  $\mathbf{F}^{(lk)}$  the force on particle  $l$  exerted by particle  $k$ .

Defining  $c$  as the semi-axis on the symmetry axis and  $a$  as the other semi-axis, see depiction in Figure 1, we define the aspect ratio  $\alpha \equiv c/a$  and the shape ratio  $r_g \equiv (c - a)/(c + a)$ . So for prolate rice-like spheroids  $\alpha > 1$ ,  $r_g > 0$  while for oblate lentil-like ones  $\alpha < 1$ ,  $r_g < 0$ . In quasi-2D flow simulations with 3D particles, it is useful to compare results at the same  $|r_g|$ , for both elongated and flattened particles. When the axis of symmetry lies in the  $xy$ -shear plane, spheroids with inverse shape ratios  $r_{g,1} = -r_{g,2}$ , or equivalently  $\alpha_1 = 1/\alpha_2$ , correspond to the same 2D ellipse within that plane, so that a direct comparison between the two is warranted.

The normal stress  $\sigma_{yy} = -P$  fluctuates around a desired target piston pressure  $P_t$  by shrinking the box in the direction of the velocity gradient with a proportional controller. The target pressure is set to ensure rigid grain behavior

\*e-mail: jacopo.bilotto@epfl.ch

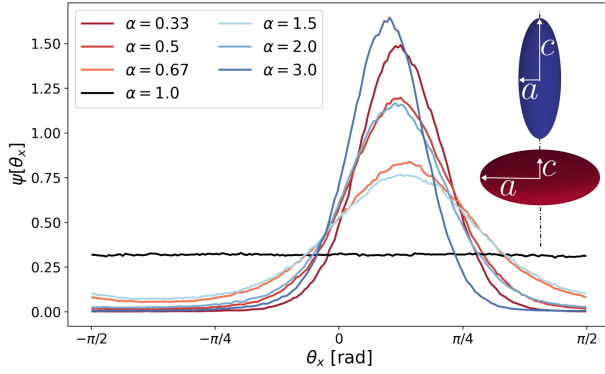


**Figure 1.** Probability density distribution of the angle between major axis of the spheroid projected in the  $xy$  plane and the  $x$  axis,  $\theta_x$ . (Inset) Representation of an elongated (blue) and flattened (red) spheroid.

with a contact stiffness number value greater than  $10^3$  [16]. The relevant dimensionless number is the inertial number  $I = \dot{\gamma} d_{eq} \sqrt{\rho_p / P}$ , where  $\dot{\gamma}$  is the shear rate,  $d_{eq} = 2a\alpha^{1/3}$  the equivalent sphere diameter. The systems are initialized at a volume fraction of  $\phi = 0.4$  by randomly distributing the particles in the simulation cell, followed by normal compression to the target pressure.

The system was then pre-strained for either 4 (low  $I$ ) or 6 strain units ( $I \geq 0.01$ ) and steady-state data were collected over at least another 10 strains. The coefficient of restitution was set to  $e = 0.1$ , the friction coefficient to  $\mu_p = 0.4$ , and the Poisson's ratio to  $\nu = 0.3$ .

We study particle shapes with  $\alpha \in [0.33, 3.0]$ , and inertial numbers  $I \in [10^{-3}, 10^{-1}]$ . Unless stated otherwise, reported quantities are averaged over all particles in steady-state conditions.

### 3 Results

Figure 1 shows that spheroids are preferentially aligned along the flow direction, with a slight tilt towards the extensional flow axis. The more elongated or flattened the particles are, the more peaked the distribution becomes.

Figure 2a and 2b display the best fits for the effective friction  $\mu(I) = \sigma_{xy}/P$ , and volume fraction  $\phi(I)$  with respect to the rheology developed in [11]:

$$\mu(I) = \mu_c + \frac{c_\mu}{1 + I_0/I} \quad (2)$$

$$\phi(I) = \phi_c - c_\phi I^{\beta_\phi}, \quad (3)$$

where  $\mu_c$ ,  $\phi_c$  are the critical effective friction and packing fraction respectively, while  $I_0$ ,  $c_\mu$ ,  $c_\phi$  are constants and  $\beta_\phi$  is a dimensionless exponent.

The volume fraction decreases as the inertial number increases, but for non-spherical particles this reduction is significantly smaller. In addition,  $\phi$  shows a non-monotonic trend with shape ratio: slightly non-spherical particles attain higher densities than more elongated or flattened ones. Remarkably, lentil-like particles reach lower densities than rice-like ones for the same value of  $|r_g|$ , across the entire range of  $I$  we studied.

Looking carefully at Figure 2c one notices that the coordination number,  $Z$ , decreases in a manner similar to the

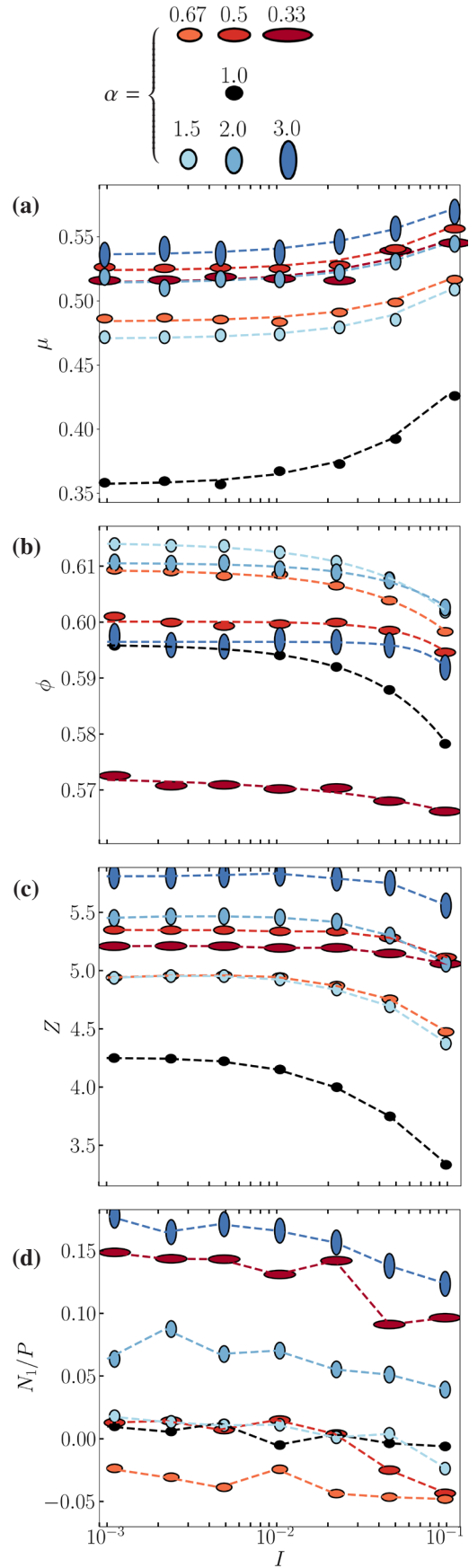


**Figure 2.** (a) Best-fit  $\mu(I)$  from Equation 2, (b) best-fit  $\phi(I)$  from Equation 3, (c) average number of contacts per particle, (d) normalized first normal stress difference. Same color legend as in Figure 1. Data points corresponding to various aspect ratios are symbolized with various ellipses (see the header of the figure).

packing fraction, although it shows an increasing monotonic trend with  $\alpha$  for elongated particles, but a non-monotonic one for flattened ones. Oblate particles have fewer contacts than prolate ones at high asphericity, as reflected also by the lower volume fraction. This can be attributed to the lower curvature of flattened particles, which allows contacts to stabilize rotational degrees of freedom more easily [17].

The same non-linearity is observed for the effective friction,  $\mu(I)$  Figure 2b: slightly flattened particles ( $|r_g| < 0.3$ ) are harder to shear than slightly elongated ones, whereas highly non spherical ones exhibit the opposite trend. The reason why non-spherical particles have a higher resistance to shear lies in their superior friction mobilization, see Figure 3b and the following discussion. Finally, the first normal stress difference,  $N_1 = \sigma_{xx} - \sigma_{yy}$ , Figure 2d, shows a weakly decreasing trend with the inertial number. For spherical particles  $N_1 \approx 0$ , whereas it grows monotonically for elongated particles, while it is non-monotonic for oblate ones, attaining negative values at low asphericity. The reason for a negative  $N_1$  is not trivial and it implies shear contraction in the flow direction, instead of the dilation common for granular materials.

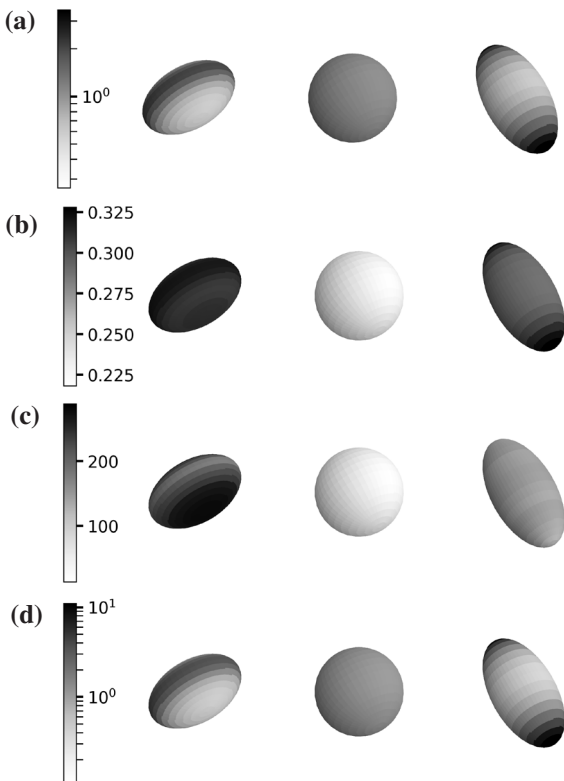


**Figure 3.** (a) Surface density of contacts times the total surface area ( $\rho_s A_p$ ), (b) friction mobilization ( $M$ ), (c) ratio of tangential to normal power dissipation, (d) power dissipation inhomogeneity, for selected shapes of spheroids. All data is measured at  $I \approx 10^{-2}$ .

Next we move on to analyze particle level data. We accumulate all interactions on the surface of a reference spheroid, neglecting the small change in size between them, due to polydispersity [10]. Calling  $\psi \in (-\pi/2, \pi/2)$  the polar angle of the spheroid, thanks to symmetry in  $\pm\psi$ ,

we bin the interaction data on surface slices at constant intervals of  $\psi$  and then collapsing it within the range  $[0, \pi/2]$ . Defining  $\rho_s$  the surface density of contacts so that  $\int_{A_p} \rho_s dA = 1$ , with  $A_p$  being the particle surface area, we observe in Figure 3a, how contacts are more likely to occur on the major axis/axes for non-spherical particles. At that same location friction is mobilized the most, i.e.  $M = F_t/F_n \implies M/\mu_p < 1$  attains its highest value, see Figure 3b. In general, non-spherical particles mobilize their frictional contacts significantly more than spherical ones in the dense regime. A likely explanation is that tangential forces between particles initially cause elastic shear loading. Spherical particles can easily rotate in response to these forces, relieving the tangential stress before substantial slip occurs. In contrast, the geometry of non-spherical particles restricts their ability to rotate freely, resulting in greater shear buildup and, consequently, increased friction mobilization. Furthermore, non-spherical particles typically form more contacts, which amplifies this effect even further.

We can split the dissipated power into a collisional term due to contact inelasticity,  $\mathcal{P}_n$ , and a tangential term due to frictional sliding  $\mathcal{P}_t$ . In Figure 3c we show that the ratio of tangential to normal power dissipation is significantly higher than the mobilized friction. Unexpectedly, tangential power dissipation outweighs normal one more strongly along the minor axis, suggesting that where there are fewer contacts ( $\rho_s$  is lower), those are more likely to occur with a smaller relative normal velocity compared to tangential. Interestingly, oblate particles dissipate more power due to friction compared to prolate ones, despite having a similar value of  $M$ .

Then, we compute the spatial inhomogeneity of power dissipation density as

$$\rho_s \mathcal{P}_j \frac{A_p}{A_j} \cdot \frac{A_p}{\mathcal{P}_p} = \frac{\rho_s \mathcal{P}_j A_p^2}{(\mathcal{P}_p A_j)}, \quad (4)$$

where  $\mathcal{P}_j$  is the average power dissipated on the surface area element  $A_j$  conditional to a contact being present, and  $\mathcal{P}_p$  is the total average power dissipated on the particle surface. Figure 3d shows that the dissipation clusters along the major axis, analogously to the number of contacts. This observation highlights the crucial role of particle geometry in energy dissipation within the system, primarily through weak grazing contacts along the major axis rather than strong sticking contacts along the minor axis.

Finally, we split the stress tensor in its normal and tangential component  $\boldsymbol{\sigma} = \boldsymbol{\sigma}_n + \boldsymbol{\sigma}_t$ , computed as in Equation 1, with exclusively the normal and tangential components of the contact force respectively. Figure 4 shows the dependence of the two components of shear stress on the aspect ratio. Although normal forces are mainly the ones generating the shear stress for spherical particles, the contribution of tangential forces increases with both elongation and flattening. Interestingly, for high values of  $|r_g|$  the total shear strength approaches saturation for prolate particles [10] and even declines for oblate ones. Therefore, despite the increase in tangential forces, the decrease in

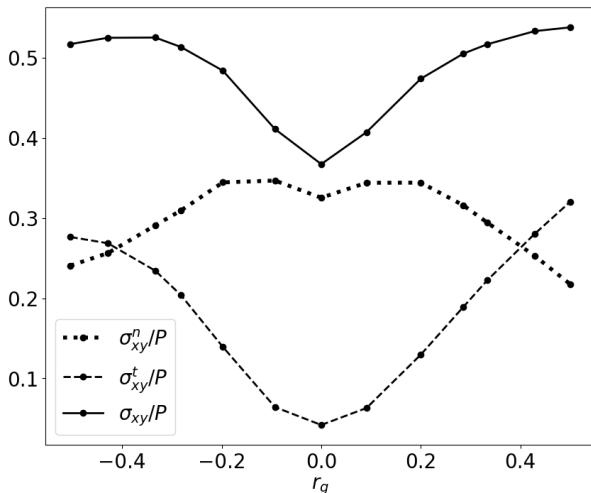


**Figure 4.** Normalized normal (dotted) and tangential (dashed) components of the shear stress, together with the total shear stress (full) at  $I = 10^{-2}$

normal loads carrying the shear limits the total rigidity of the system. Given a fixed value of  $\mu_p$ , the maximum shear strength is thus obtained at a finite value of  $\alpha$ .

#### 4 Discussion and Conclusions

Our study shows that particle shape strongly influences dense granular flows, affecting density, contact network, and energy dissipation. Non-spherical particles align with the flow, with moderate shape anisotropy leading to higher volume fractions, whereas extreme elongation or flattening reduces it.

Effective friction also follows a non-monotonic trend: slightly flattened particles resist shear more than elongated ones, but at high asphericity, the trend reverses. Power dissipation clusters on the major axis, which is roughly oriented along the streamlines. Additionally, tangential forces play a larger role in shear resistance for non-spherical grains, yet beyond a critical shape ratio, shear strength saturates or declines.

This work opens opportunities for additional research on industrial machines that handle and process grains and pills. Future work could explore frictional and cohesive effects, as well as flows with polydispersity of shapes and their segregation. The data presented here could be used to inform more complex rheological models and the effect of the full 3D shape should also be investigated in shear reversal [18].

#### 5 Acknowledgments

This project has received funding from the European Union's Horizon 2020 research and innovation programme under the Marie Skłodowska-Curie grant agreement No 945363. We also acknowledge financial support from Bühler AG.

#### References

[1] E. Azéma, F. Radjai, Stress-strain behavior and geometrical properties of packings of elongated particles, *Physical Review E* **81**, 051304 (2010).

[2] T. Börzsönyi, R. Stannarius, Granular materials composed of shape-anisotropic grains, *Soft Matter* **9**, 7401 (2013).

[3] M. Botton, E. Azéma, N. Estrada, F. Radjai, A. Lizcano, Quasistatic rheology and microstructural description of sheared granular materials composed of platy particles, *Physical Review E* **87**, 032206 (2013).

[4] C.S. Campbell, Granular shear flows at the elastic limit, *Journal of fluid mechanics* **465**, 261 (2002).

[5] C.S. Campbell, Elastic granular flows of ellipsoidal particles, *Physics of Fluids* **23** (2011).

[6] Y. Guo, C. Wassgren, W. Ketterhagen, B. Hancock, B. James, J. Curtis, A numerical study of granular shear flows of rod-like particles using the discrete element method, *Journal of fluid Mechanics* **713**, 1 (2012).

[7] Y. Guo, C. Wassgren, B. Hancock, W. Ketterhagen, J. Curtis, Granular shear flows of flat disks and elongated rods without and with friction, *Physics of Fluids* **25** (2013).

[8] M. Trulsson, Rheology and shear jamming of frictional ellipses, *Journal of Fluid Mechanics* **849**, 718 (2018).

[9] D.B. Nagy, P. Claudin, T. Börzsönyi, E. Somfai, Flow and rheology of frictional elongated grains, *New Journal of Physics* **22**, 073008 (2020).

[10] Y. Zou, G. Ma, S. Zhao, S. Chen, W. Zhou, Particle shape transforms the driving of shear stress in granular materials, *Powder Technology* **416**, 118235 (2023).

[11] P. Jop, Y. Forterre, O. Pouliquen, A constitutive law for dense granular flows, *Nature* **441**, 727 (2006).

[12] B. Nadler, F. Guillard, I. Einav, Kinematic model of transient shape-induced anisotropy in dense granular flow, *Physical review letters* **120**, 198003 (2018).

[13] B. Nadler, Anisotropic inertia rheology of ellipsoidal grains, *Granular Matter* **23**, 14 (2021).

[14] C. Goniva, C. Kloss, A. Hager, S. Pirker, An open source CFD-DEM perspective, in *Proceedings of OpenFOAM Workshop, Göteborg* (2010), pp. 22–24

[15] A. Podlozhnyuk, S. Pirker, C. Kloss, Efficient implementation of superquadric particles in Discrete Element Method within an open-source framework, *Computational Particle Mechanics* **4** (2016).

[16] F. Da Cruz, S. Emam, M. Prochnow, J.N. Roux, F. Chevoir, Rheophysics of dense granular materials: Discrete simulation of plane shear flows, *Physical Review E* **72**, 021309 (2005).

[17] A. Donev, I. Cisse, D. Sachs, E.A. Variano, F.H. Stillinger, R. Connelly, S. Torquato, P.M. Chaikin, Improving the density of jammed disordered packings using ellipsoids, *Science* **303**, 990 (2004).

[18] M. Trulsson, Directional shear jamming of frictionless ellipses, *Physical Review E* **104**, 044614 (2021).